

# Impact-activated solidification of dense suspensions via dynamic jamming fronts

Scott R. Waitukaitis<sup>1</sup> & Heinrich M. Jaeger<sup>1</sup>

Although liquids typically flow around intruding objects, a counterintuitive phenomenon occurs in dense suspensions of micrometre-sized particles: they become liquid-like when perturbed lightly, but harden when driven strongly<sup>1–5</sup>. Rheological experiments have investigated how such thickening arises under shear, and linked it to hydrodynamic interactions<sup>1,3</sup> or granular dilation<sup>2,4</sup>. However, neither of these mechanisms alone can explain the ability of suspensions to generate very large, positive normal stresses under impact. To illustrate the phenomenon, such stresses can be large enough to allow a person to run across a suspension without sinking, and far exceed the upper limit observed under shear or extension<sup>2,4,6,7</sup>. Here we show that these stresses originate from an impact-generated solidification front that transforms an initially compressible particle matrix into a rapidly growing jammed region, ultimately leading to extraordinary amounts of momentum absorption. Using high-speed videography, embedded force sensing and X-ray imaging, we capture the detailed dynamics of this process as it decelerates a metal rod hitting a suspension of cornflour (cornstarch) in water. We develop a model for the dynamic solidification and its effect on the surrounding suspension that reproduces the observed behaviour quantitatively. Our findings suggest that prior interpretations of the impact resistance as dominated by shear thickening need to be revisited.

To produce significant shear or normal stresses, current explanations for the hardening observed in driven suspensions all require some confinement, via the presence of walls or boundaries. In models based on liquid-mediated formation of particle clusters<sup>3,8</sup>, the clusters need to percolate between the shearing walls<sup>9</sup>, and in models treating dense suspensions as granular, frictional fluids<sup>4,10,11</sup> dilation must be counteracted by confinement, similar to “shear-jamming”<sup>12</sup> in dry, granular systems. The upper limit of (normal or shear) stresses under steady-state shearing is then set by the stiffness of the particles or the boundary, whichever is more compliant<sup>4,13,14</sup>. In prototypical suspensions of hard particles such as cornflour in water, compliance of the interface with the surrounding air limits the stresses to no more than 5–10 kPa under shear or extension<sup>2,4,6,7</sup>. The requirement for stiff boundaries is also problematic because strong shear thickening is also observable in large containers where poking (or stepping on) the suspension hardens it locally but leaves most of its volume in a liquid-like state. Two recent experiments suggest that jammed regions transmit stresses to the container bottom<sup>15,16</sup>, but do not address how these regions form. Using a large suspension volume (25 litres) to avoid boundaries and to enable tracking of the growth of such regions with precision, we show here that stresses in the megapascal range can be generated dynamically without requiring confinement or proximity to hard surfaces.

Figure 1 shows images before and after an aluminium rod strikes a dense suspension of cornflour and water (see Supplementary Movie 1). Rather than penetrating the surface, the rod pushes it down, causing a rapidly growing depression whose boundary travels away from the impact site. This immediately sets the medium apart from water or grains alone, where impact is generally accompanied by splashing<sup>17,18</sup>

and where the impactor penetrates significantly. We plot the rod’s instantaneous acceleration ( $a_{\text{rod}}$ ), velocity ( $v_{\text{rod}}$ ), and position ( $z_{\text{rod}}$ ) versus time  $t$  in Fig. 1e. The acceleration is characterized by a pronounced peak  $a_{\text{peak}}$  occurring at time  $t_{\text{peak}}$ . The scale of this peak at a given impact velocity is typically about a hundred times larger than for water alone<sup>19</sup>, with decelerations as high as 100g (where  $g$  is the acceleration due to gravity) and pressures on the bottom face of the rod exceeding 1 MPa. At times much larger than  $t_{\text{peak}}$ , the impacting object, now nearly stationary, begins slowly to sink. In the following we focus on the early-time behaviour before this sinking and on the velocity regime  $0.2 < v_0 < 2 \text{ m s}^{-1}$ , beyond which this material fails and the rod begins to penetrate the surface. We used cornflour/water mixtures as a model suspension because of its pronounced impact hardening and the ready availability of large quantities, but we expect similar behaviour with other types of dense suspensions<sup>2</sup>.

The existence of peaks in  $a_{\text{rod}}$  versus  $t$  suggests that the force exerted on the rod by the suspension is a competition between time-increasing and time-decreasing contributions. One of these is related to  $v_{\text{rod}}$  (Fig. 1f) as increasing  $v_0$  causes  $a_{\text{peak}}$  to grow from about 1g to 100g and  $t_{\text{peak}}$  to shrink. Raising the packing fraction  $\phi$  (the ratio of total particle volume to system volume) by even a small amount led to a considerably stronger impact response (about twice as large for  $\phi = 0.46$  to 0.52), but preserves the shape of the curves shown in Fig. 1. Although the response depends strongly on the grain packing fraction, it is surprisingly insensitive to the fluid parameters. By adding a ~1-cm-deep layer of water to the suspension surface and thereby effectively setting the surface tension  $\gamma$  to zero, we see that the response is not a consequence of particles dilating into the liquid–air interface, as is observed in steady-state shear experiments<sup>2</sup>. Mixing the water with glycerol and increasing its viscosity  $\eta$  by more than a factor of ten changes neither the shape of the acceleration curves nor the height and time of the peaks, even though it strongly slows the rod’s steady-state sinking after impact.

To understand the role of boundaries, we changed the suspension depth  $H$  (Fig. 2a). For the deepest suspension,  $a_{\text{peak}}$  occurs at  $t_{\text{peak}} \approx 10 \text{ ms}$ , but a second, weaker peak is just visible near  $t \approx 75 \text{ ms}$ . Lowering  $H$  causes this peak to intensify and move to earlier times. For the smallest  $H$  a third peak emerges, resulting from a second impact of the rod after a subtle bounce. This second peak does not arise from transmitted and reflected waves, but is the signature of solidification suspected by Liu *et al.*<sup>16</sup> and von Kann *et al.*<sup>15</sup>. To verify this, we simultaneously measured the force  $F_b$  transmitted to the bottom boundary with an immersed force sensor (Fig. 2a). Whereas almost no force is measured at  $t_{\text{peak}}$ ,  $F_b$  strongly correlates with peaks two and three. This has many important implications: first, the primary response is not the result of stress transmission to the boundary; second, the solidification process requires a finite amount of time to propagate through the suspension; third, once solidification reaches the bottom boundary, forces propagate with no detectable delay through a now jammed, solid-like region back towards the impactor; and fourth, this jammed solid can bear stress and store energy, allowing, for example, the bounce of the impactor. We can thus interpret the second peak in

<sup>1</sup>James Franck Institute and Department of Physics, The University of Chicago, Chicago, Illinois 60637, USA.

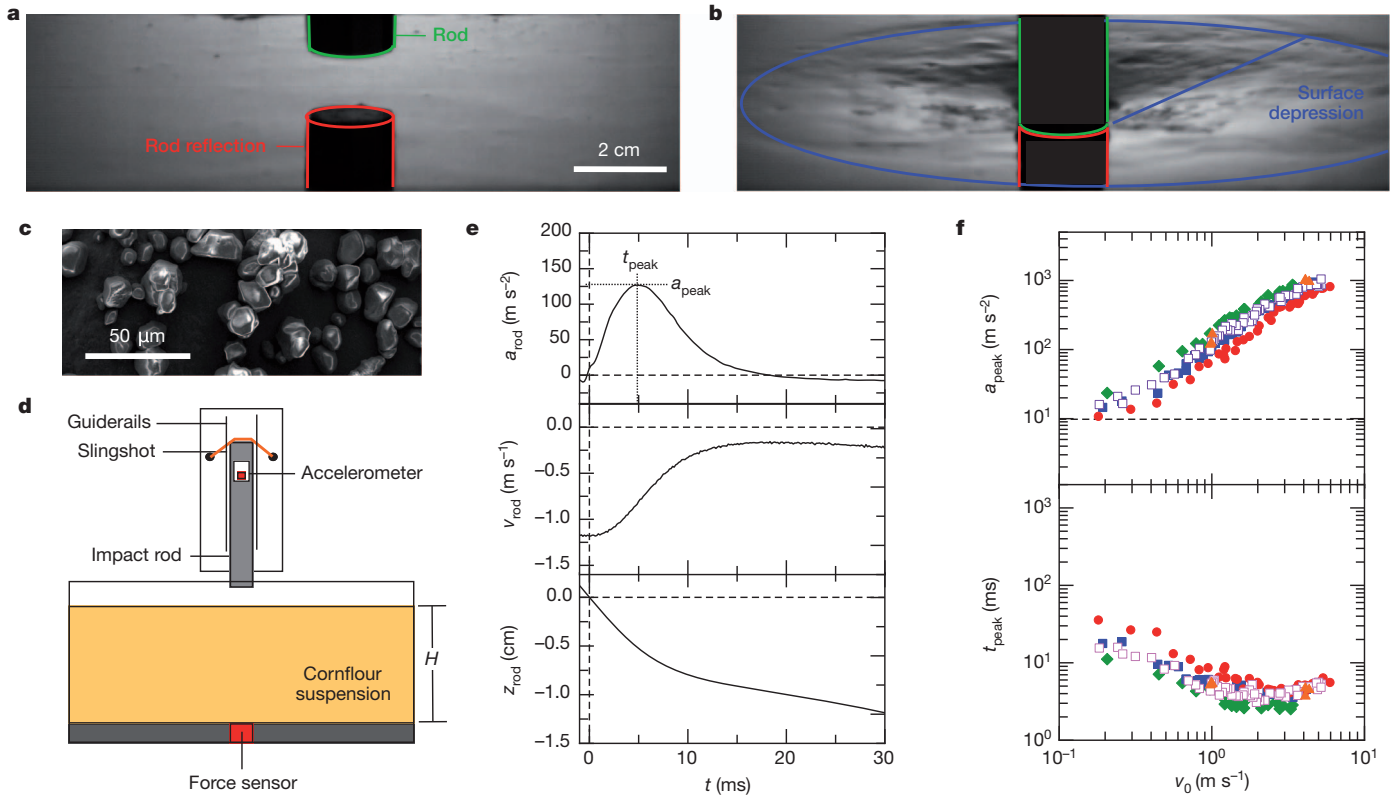


**Figure 1 | Impact into a cornflour and water suspension.** Images of an aluminium rod ( $r_{\text{rod}} = 0.93$  cm,  $m_{\text{rod}} = 0.368$  kg) before (a) and about 15 ms after (b) striking the surface of the cornflour/water suspension ( $\phi = 0.49$ ,  $\eta = 1$  cP) at  $v_0 \approx 1$  m s $^{-1}$ . The rod and its reflection are outlined in green and red respectively, for clarity. A large depression develops radially from the impact site (outlined in blue). For the full evolution, see Supplementary Movie 1. c, Scanning electron microscope image of dried cornflour grains extracted from the suspension after experiments. Grains are irregularly shaped with diameters  $d \approx 5$ – $20$   $\mu\text{m}$ . No differences are visible between grains imaged before and after experiments. d, The rod is housed by guiderails and launched via free-fall or slingshot. Instantaneous rod acceleration is measured with an embedded accelerometer; high-speed video (Phantom v9.1, around 10,000 frames per second) gives access to independent position and velocity measurements and, with a laser line (not shown), the dynamic surface profile of

$a_{\text{rod}}$  as occurring at the time  $t_{\text{front}}$  required for the front of a developing solid to reach bottom. Figure 2b shows  $t_{\text{front}}(H)$  for two different impact velocities  $v_0$ . Using these data to compute the travel distance of the front  $h_{\text{front}} = H - h_{\text{rod}}$  and plotting this against the travel distance of the rod ( $h_{\text{rod}} = |z_{\text{rod}}|$  at  $t_{\text{front}}$ ), we find nearly linear collapse, that is,  $h_{\text{front}} = kh_{\text{rod}}$  with  $k = 12.2 \pm 0.1$ . This establishes that the solid growth is driven by the rod's motion, with the solidification front moving ahead of the rod at velocity  $v_{\text{front}} = kv_{\text{rod}}$ .

This behaviour conjures images of granular shocks<sup>20</sup> or solidification fronts in supercooled glass-forming liquids<sup>21–23</sup>. With granular shocks, however, the front propagates through an already-jammed medium and its speed is governed by elastic energy stored in grains<sup>20</sup>. Although supercooled liquids, like the system here, are initially unjammed, their solidification fronts propagate at a constant, thermodynamically favoured speed<sup>24</sup>. Here solidification is more reminiscent of a snowplough, as illustrated in Fig. 2g. In this picture, hard, highly dissipative grains of diameter  $d$  have initial interstitial spacing  $\delta$ . Pushing this arrangement with speed  $v_{\text{rod}}$  creates a solidification front moving (relative to the rod) with velocity  $v_{\text{front}} = v_{\text{rod}}d/\delta$ , which after integration leads to  $h_{\text{front}} = kh_{\text{rod}}$ , with  $k = d/\delta$ . Dry cornflour grains themselves are not perfectly inelastic, but their interactions in suspension are mediated by lubrication forces. These depend strongly on the relative velocity  $v_{\text{rel}}$  of the grains ( $F = 3\pi\eta d^2 v_{\text{rel}}/8\delta$  for head-on

the suspension (see Fig. 2d–f). An immersed force sensor records stress transmission to the lower boundary directly below the rod. e, Rod acceleration  $a_{\text{rod}}$ , velocity  $v_{\text{rod}}$  and position  $z_{\text{rod}}$  versus time  $t$  for  $v_0 = 1.18$  m s $^{-1}$ . Acceleration curves reach a peak  $a_{\text{peak}}$  at time  $t_{\text{peak}}$ , indicating a competition in the force law. f, Measurements of  $a_{\text{peak}}$  and  $t_{\text{peak}}$  versus  $v_0$  for suspending fluid viscosity  $\eta = 1$  cP and  $\phi = 0.46$  (red circles),  $0.49$  (blue squares), and  $0.52$  (green diamonds),  $\eta = 12.4$  cP and  $\phi = 0.49$  (open purple squares), and  $\eta = 1$  cP and  $\phi = 0.49$  with a water layer about 1 cm deep on the surface (orange triangles). The insensitivity to  $\eta$  shows that the impact response has little dependence on the suspension's effective steady-state viscosity, while the addition of the water layer shows that the response is not mediated by the surface-tension stress associated with particles dilating through the liquid–air interface. The data in Figs 2 and 4 correspond to  $\phi = 0.49$  and  $\eta = 1$  cP, and the data in Fig. 3 correspond to  $\phi = 0.49$  and  $\eta \approx 7$  cP.

collisions<sup>25,26</sup>), leading to significant dissipation even before contact. Despite the viscosity dependence, grains aligned as in Fig. 2d but surrounded by fluid produce front speeds simply set by geometry because little energy storage is present (see Supplementary Information). From the experimental value for  $k$  in Fig. 2c this scenario suggests an interstitial gap  $\delta$  of the order of  $d/12.2 \approx 1$   $\mu\text{m}$ , a realistic value for the dense suspensions used.

This clarifies how solidification can develop in one dimension, but the system considered is three-dimensional. Furthermore, while  $\phi$  can change locally, the suspension is globally incompressible, and  $\nabla \cdot \mathbf{v} \approx 0$  must hold system-wide (changes in  $\rho$  are negligible). The surface depression (Fig. 1a, b) arises from this constraint. As grains below move rigidly with the rod, they pull on their neighbours, causing the surrounding suspension to move down, too. High-speed video of a laser line projected onto the suspension–air interface (stills in Fig. 2d and e; see Supplementary Movie 2 for the full evolution) allowed us to capture this quantitatively in space–time plots of the surface depression  $h_{\text{surf}}$  versus time  $t$  and radial coordinate  $r$ , shown in Fig. 2f. The contour for  $h_{\text{surf}} = 0$  shows that the radial extent of the depression slows with the rod, just like the solid front below. We demonstrated this directly by overlaying the distance of the solid front beyond the rod,  $z_{\text{front}}$  (obtained from  $z_{\text{front}} = k|z_{\text{rod}}|$  with  $k = 12.2$ ), onto the space–time plot. This shows that although compressive jamming of

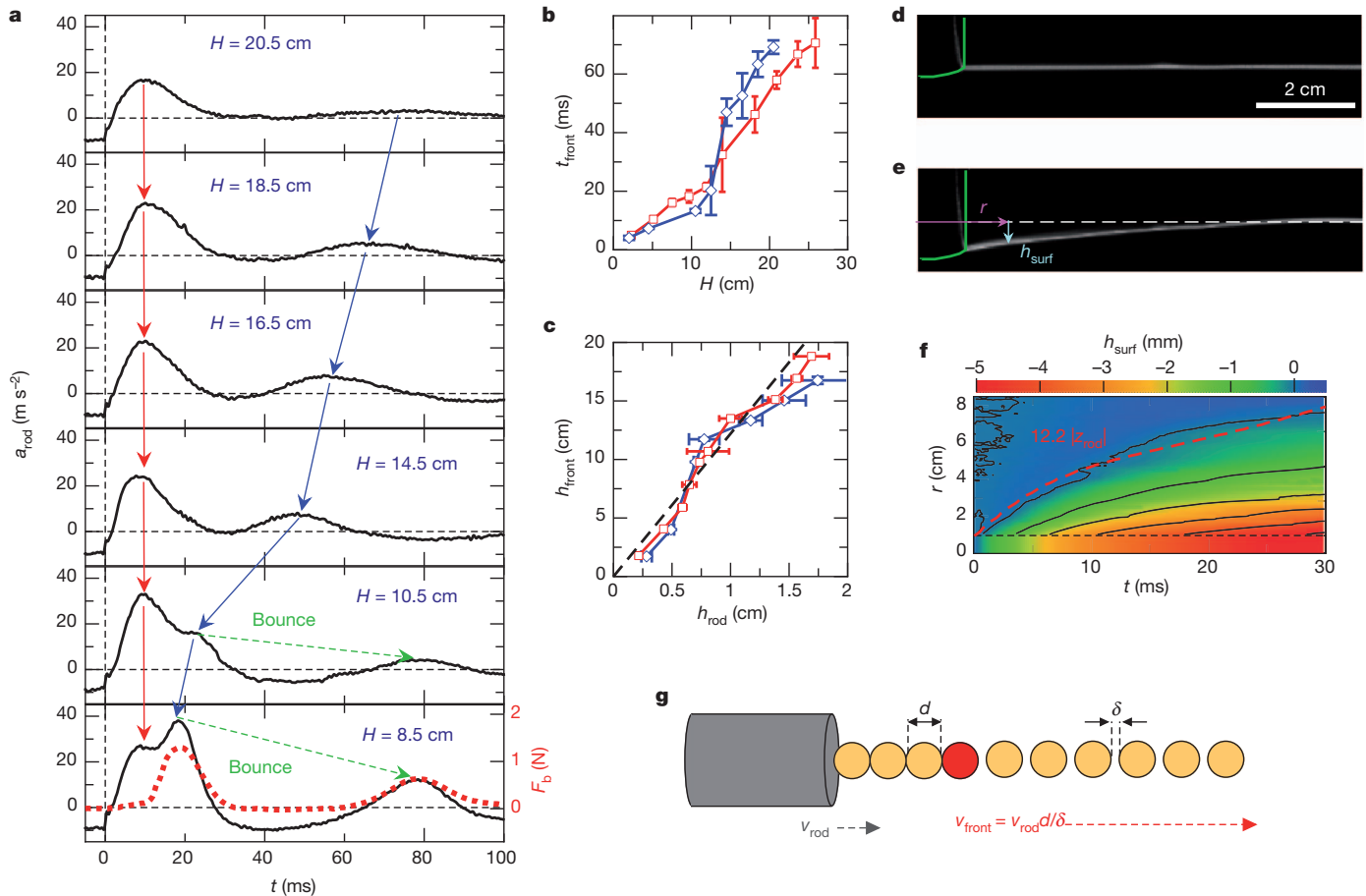


**Figure 2 | Suspension solidification and surface dynamics.** **a**,  $a_{\text{rod}}$  versus  $t$  for  $v_0 = 0.49 \pm 0.04 \text{ m s}^{-1}$  and various  $H$  values as shown. The first peak ( $t_{\text{peak}} \approx 10 \text{ ms}$ ) is the same as described in Fig. 1 and is largely independent of  $H$ . A subsequent, second peak is strongly affected by  $H$ , moving to earlier times and increasing as  $H$  decreases. This peak arises from solid-like stress transmission between the rod and container bottom, as confirmed by the correlated peaks in the force  $F_b$  measured at the container bottom overlaid for the  $H = 8.5 \text{ cm}$  trial (the third peak at  $t \approx 80 \text{ ms}$  results from a subsequent impact after a subtle bounce). The time of the second peak is interpreted as the time  $t_{\text{front}}$  required for the front of a solidified region to reach the bottom. **b**, Solid front time-of-flight measurements  $t_{\text{front}}$  versus  $H$ . Red squares and blue diamonds correspond to  $v_0 = 0.49 \pm 0.04 \text{ m s}^{-1}$  and  $0.9 \pm 0.1 \text{ m s}^{-1}$ , respectively. The error bars represent the standard deviation from five

individual measurements. **c**,  $h_{\text{front}} = H - h_{\text{rod}}$  versus  $h_{\text{rod}} = |z_{\text{rod}}|$  at  $t_{\text{front}}$ . The dashed line is for  $h_{\text{front}} = kh_{\text{rod}}$  with  $k = 12.2 \pm 0.1$ . Symbols and error bars are as in **b**. Images of laser line on suspension surface at times just before (**d**) and about 15 ms after (**e**) impact (see Supplementary Movie 2 for full evolution). **f**, Space-time plot of surface depression  $h_{\text{surf}}$  (colour field) versus time  $t$  (horizontal axis) and radius  $r$  (vertical axis) for  $v_0 = 0.49 \pm 0.01 \text{ m s}^{-1}$ . The dashed black line indicates the boundary between rod and suspension. The solid red line indicates front trajectory  $z_{\text{front}} = 12.2|z_{\text{rod}}|$  measured relative to rod, which closely follows the maximum extent of depression (where  $h_{\text{surf}} = 0 \text{ mm}$ ). **g**, Cartoon of particulate-phase snowplough. A line of highly dissipative grains (diameter  $d$ , interstitial spacing  $\delta$ ) pushed with speed  $v_{\text{rod}}$  solidifies at a rate  $v_{\text{front}} = v_{\text{rod}}d/\delta$  (measured relative to the rod).

the particulate phase can only occur below the rod, significant momentum transfer also occurs to the surrounding suspension as it is compelled to move downward.

To see this better, we looked inside the optically opaque suspension with X-ray videography (Supplementary Movie 3), loading it with high-contrast tracer particles and using particle image velocimetry (PIV) to calculate the displacement field resulting from the impact (our X-ray setup requires a smaller suspension volume than used for Figs 1 and 2, but the salient features remain the same—see Supplementary Discussion II). The displacement field (Fig. 3a) shows a large region below the rod that is pushed primarily downward; this is visual evidence of the jammed solid and the surrounding suspension that have absorbed the rod's momentum. Just outside this yellowish region, the field curls outward and upward to conserve volume globally.

For the jammed region directly below the rod ( $z < 0$ ,  $r < r_{\text{rod}}$ ) we can use the simplified one-dimensional model to predict the magnitude of the vertical displacements  $|\Delta z|$ . A grain at  $z$  (Fig. 3e) is assumed to be motionless until the front reaches it. The front and rod positions are related by  $z_{\text{front}} = k|z_{\text{rod}}|$  (with  $z_{\text{front}}$  measured relative to the rod) and  $|z| = |z_{\text{rod}}| + z_{\text{front}}$ , so this happens when  $|z_{\text{rod}}| = |z|/(k+1)$ .

Afterwards, the grain moves with the rod. Thus, if the rod moves a total distance  $h_{\text{rod}}$  between the two X-ray images, the grain moves  $|\Delta z| = h_{\text{rod}} - |z_{\text{rod}}| = h_{\text{rod}} - |z|/(k+1)$ , whereas beyond  $|z| = h_{\text{rod}}/(k+1)$  we expect  $|\Delta z| = 0$ . Fitting this form to the data for  $|\Delta z|$  obtained from the X-rays (Fig. 3d) yields  $k = 13.1 \pm 0.9$ , close to the value  $k = 12.2 \pm 0.1$  obtained from the acceleration curves (Fig. 2c).

These results paint a picture in which the seed of the response is the dynamic growth of the jammed solid below the impact site. As this solid grows and is forced to move with the rod, it causes flow in the surrounding fluid. The interplay between this growing region of moving suspension and the slowing of the rod is the competition mechanism responsible for the observed peaks in the rod deceleration. We can capture the essence of this behaviour using the concept of added mass, as is frequently done for surface impact in regular liquids<sup>19,27–29</sup>. The key idea is to think of the impact as an inelastic collision with a growing mass,  $m_a$ . The rod dynamics are captured by force balance:

$$(m_{\text{rod}} + m_a)a_{\text{rod}} = -(dm_a/dt)v_{\text{rod}} + F_{\text{ext}} \quad (1)$$

where  $F_{\text{ext}}$  in our case comes from gravity ( $F_g = -m_{\text{rod}}g$ ) and the buoyant force from the displaced fluid in the depression (from

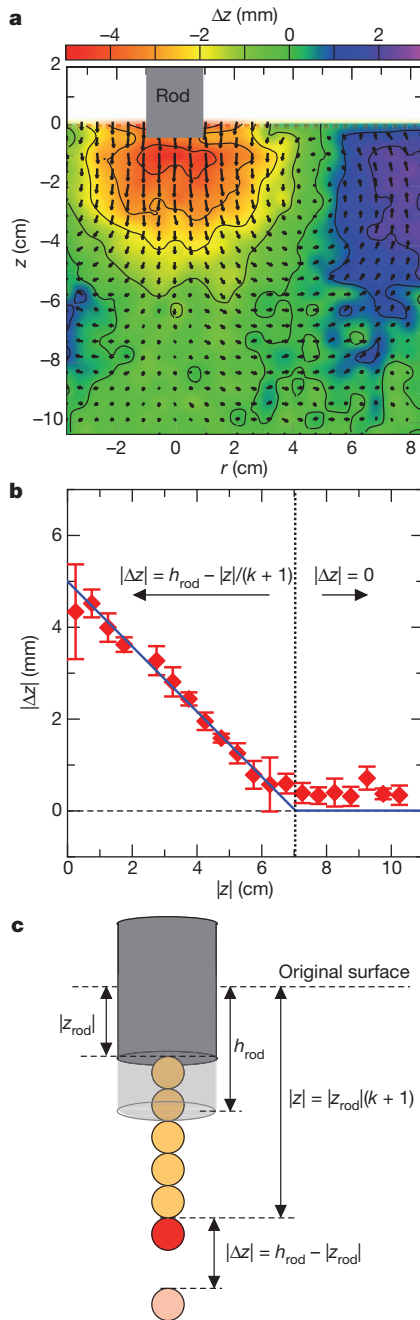


**Figure 3 | Displacement field of suspension interior during impact.** **a**, Displacement field of suspension interior calculated from averaging PIV analysis of X-ray images taken before/after impact (for apparatus and experimental details, see Supplementary Discussion II, and for the full evolution see Supplementary Movie 3). The vectors give the displacements of each point calculated over a time duration of  $\Delta t \geq 60$  ms, while the colours correspond to the vertical displacements along  $\Delta z$ . The large red/yellow region is the signature of the solidified mass and surrounding suspension that is forced downward by the rod. Outside this, the suspension behaves like an incompressible fluid and curls outward and upward to satisfy volume conservation. **b**, Data (red diamonds) versus model (blue line) for vertical displacements  $|\Delta z|$  directly below rod as a function of distance below original suspension surface  $|z|$ . The data are calculated by averaging the displacements of all points directly below the rod in bins of height 0.5 cm, and the error bars show the standard deviations of the measurements in these bins. The model fit is of the form  $|\Delta z| = h_{\text{rod}} - |z|/(k + 1)$  for  $z < h_{\text{rod}}(k + 1)$  and  $z = 0$  for  $z \geq h_{\text{rod}}(k + 1)$ , with  $k = 13.1 \pm 0.9$  and  $h_{\text{rod}} = 5.0 \pm 0.2$  mm. **c**, Cartoon illustrating the snowplough mechanism that produces the predicted form (blue curve) of the vertical displacements  $|\Delta z|$  in Fig. 3b.

Fig. 2,  $F_b \approx 1/3\pi\rho g(r_{\text{rod}} + k|z_{\text{rod}}|)^2|z_{\text{rod}}|$ ). With normal liquids,  $m_a$  is typically limited by the density of the liquid and the size of the impactor, for example,  $m_a < C(4/3)\pi\rho(r_{\text{rod}})^3$  for disk impact<sup>29</sup>. The factor  $C$  is the ‘added mass coefficient’ and accounts for the fact that the fluid does not actually move like a solid object (consequently,  $C$  is typically  $< 1$ ; ref. 27). The suspension is capable of responding so dramatically because the solidification below the rod leads to rapid, effectively unlimited, growth of  $m_a$ . We can estimate its size from Figs 2 and 3, which show that the impact creates substantial flow in a region that extends  $k|z_{\text{rod}}|$  below and radially away from the rod. Approximating these points as bounding a cone-like region gives  $m_a$  the form:

$$m_a = C(1/3)\pi\rho(r_{\text{rod}} + k|z_{\text{rod}}|)^2k|z_{\text{rod}}| \quad (2)$$

Using this in equation (1) with the initial conditions  $v_{\text{rod}}(0) = v_0$  and  $z_{\text{rod}}(0) = 0$  allows us to solve numerically for the rod dynamics.

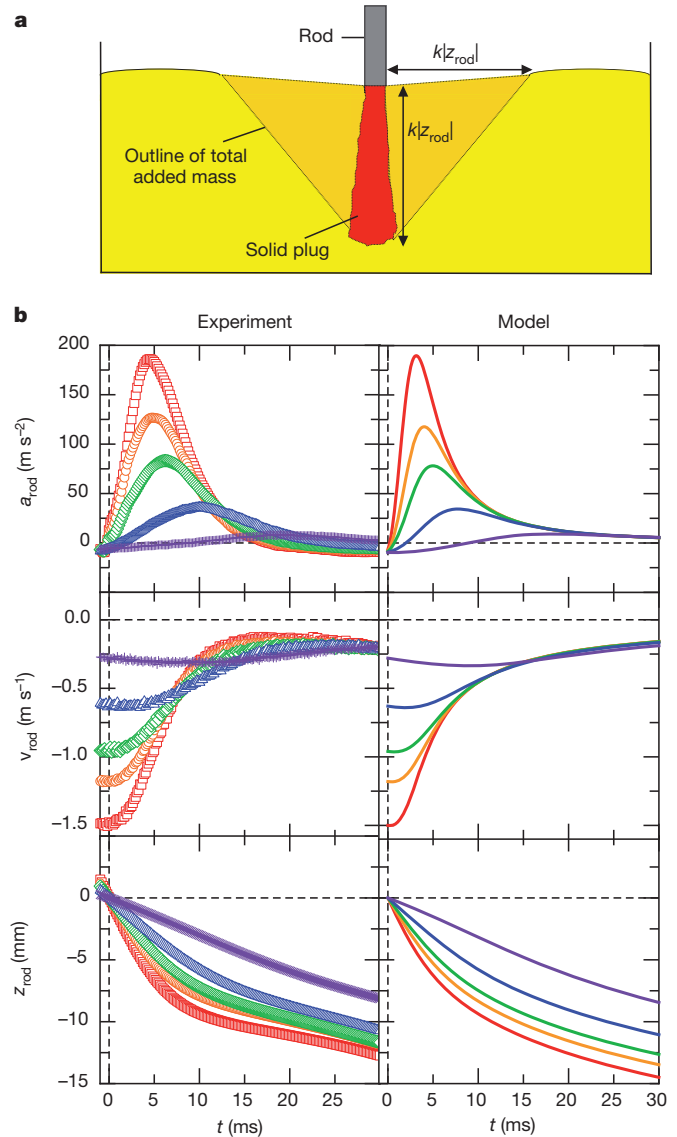


**Figure 4 | Added mass model for impact.** **a**, Illustration of the solidification below the rod and the induced flow in the suspension. The red area represents the solidified region, while the surrounding orange colour represents the effective shape of the added mass  $m_a$ , and the yellow represents the remaining suspension. **b**, Side-by-side comparison of experimental values for  $a_{\text{rod}}$ ,  $v_{\text{rod}}$  and  $z_{\text{rod}}$  versus  $t$  to the model. Impact velocities for experimental data:  $v_0 = 1.50$  m s<sup>-1</sup> (red squares), 1.18 m s<sup>-1</sup> (orange circles), 0.96 m s<sup>-1</sup> (green diamonds), 0.63 m s<sup>-1</sup> (blue triangles) and 0.28 m s<sup>-1</sup> (purple crosses). The corresponding curves for model have the same colours.

Using the average measured value  $k = 12.5$  and leaving the coefficient  $C$  as the only adjustable parameter, this minimal model reproduces both magnitude and timing of the impact response surprisingly well over the whole range of initial velocities tested (Fig. 4). We find good agreement for  $C \approx 0.37$ , similar to what is encountered for disk impact into regular liquids<sup>26</sup>. We can also extract  $m_a$  directly from our data and confirm the scaling with  $z_{rod}$  as given by equation (2) (see Supplementary Discussion III).

Although large impact resistance has in the past been taken as a prototypical example of shear-induced thickening, our findings point to a different mechanism more akin to crossing the jamming transition by compression along the packing density ( $\phi$ ) axis<sup>30</sup>. Surface impact precipitates a sudden, local compression of the particle matrix, forcing it across the jamming transition and leading to a rapidly growing solid mass whose motion drives flow in the surrounding suspension. The impact-jammed solid is transient, but before “melting”<sup>15</sup>, it exhibits a yield stress and elastic properties, in contrast to shear-thickened states that only exist beyond yielding<sup>2,11</sup>. We provide direct evidence that this solid can transmit stress between the moving object and a boundary, in agreement with previous experiments<sup>15,16</sup>. Importantly, however, we find that the critical element in creating large normal stresses during impact is not the presence of a boundary, but instead the momentum transferred as the quickly growing, jammed solid is pushed through the surrounding suspension by the impactor.

Received 5 March; accepted 1 May 2012.

- Cheng, X., McCoy, J. H., Israelachvili, J. N. & Cohen, I. Imaging the microscopic structure of shear thinning and thickening colloidal suspensions. *Science* **333**, 1276–1279 (2011).
- Brown, E. *et al.* Generality of shear thickening in dense suspensions. *Nature Mater.* **9**, 220–224 (2010).
- Wagner, N. J. & Brady, J. F. Shear thickening in colloidal dispersions. *Phys. Today* **62**, 27–32 (2009).
- Fall, A., Huang, N., Bertrand, F., Ovarlez, G. & Bonn, D. Shear thickening of cornstarch suspensions as a reentrant jamming transition. *Phys. Rev. Lett.* **100**, 018301 (2008).
- Merkt, F. S., Deegan, R. D., Goldman, D. I., Rericha, E. C. & Swinney, H. L. Persistent holes in a fluid. *Phys. Rev. Lett.* **92**, 184501 (2004).
- Bischoff White, E. E., Chellamuthu, M. & Rothstein, J. P. Extensional rheology of a shear-thickening cornstarch and water suspension. *Rheol. Acta* **49**, 119–129 (2010).
- Smith, M. I., Besseling, R., Cates, M. E. & Bertola, V. Dilatancy in the flow and fracture of stretched colloidal suspensions. *Nature Commun.* **1**, 114–115 (2010).
- Brady, J. F. & Bossis, G. Stokesian dynamics. *Annu. Rev. Fluid Mech.* **20**, 111–157 (1988).
- Maranzano, B. J. & Wagner, N. J. The effects of particle-size on reversible shear thickening of concentrated colloidal dispersions. *J. Chem. Phys.* **114**, 10514–10527 (2001).
- Brown, E. *et al.* Shear thickening and jamming in densely packed suspensions of different particle shapes. *Phys. Rev. E* **84**, 031408 (2011).
- Brown, E. & Jaeger, H. M. Dynamic jamming point for shear thickening suspensions. *Phys. Rev. Lett.* **103**, 086001 (2009).
- Bi, D., Zhang, J., Chakraborty, B. & Behringer, R. P. Jamming by shear. *Nature* **480**, 355–358 (2011).
- Cates, M. E., Haw, M. D. & Holmes, C. B. Dilatancy, jamming, and the physics of granulation. *J. Phys. Condens. Matter* **17**, S2517–S2531 (2005).
- Brown, E. & Jaeger, H. M. The role of dilation and confining stresses in shear thickening of dense suspensions. *J. Rheol.* **56**, 875–923 (2012).
- von Kann, S., Snoeijer, J. H., Lohse, D. & van der Meer, D. Nonmonotonic settling of a sphere in a cornstarch suspension. *Phys. Rev. E* **84**, 060401 (2011).
- Liu, B., Shelley, M. & Zhang, J. Focused force transmission through an aqueous suspension of granules. *Phys. Rev. Lett.* **105** (2010).
- Royer, J. R. *et al.* Formation of granular jets observed by high-speed X-ray radiography. *Nature Phys.* **1**, 164–167 (2005).
- Fedorchenko, A. I. & Wang, A. B. On some common features of drop impact on liquid surfaces. *Phys. Fluids* **16**, 1349–1365 (2004).
- Moghisi, M. & Squire, P. T. An experimental investigation of the initial force of impact on a sphere striking a liquid surface. *J. Fluid Mech.* **108**, 133–146 (1981).
- Gómez, L. R., Turner, A. M., van Hecke, M. & Vitelli, V. Shocks near jamming. *Phys. Rev. Lett.* **108**, 058001 (2012).
- Debenedetti, P. G. & Stillinger, F. H. Supercooled liquids and the glass transition. *Nature* **410**, 259–267 (2001).
- Papoular, M. Dense suspensions and supercooled liquids: dynamic similarities. *Phys. Rev. E* **60**, 2408–2410 (1999).
- Ediger, M. D., Angell, C. A. & Nagel, S. R. Supercooled liquids and glasses. *J. Phys. Chem.* **100**, 13200–13212 (1996).
- Graham, D. J., Magdolinos, P. & Tosi, M. Investigation of the solidification of benzophenone in the supercooled liquid state. *J. Phys. Chem.* **99**, 4757–4762 (1995).
- Hocking, L. M. The effect of slip on the motion of a sphere close to a wall and of two adjacent spheres. *J. Eng. Math.* **7**, 207–221 (1973).
- Davis, R. H. & Serayssol, J.-M. The elastohydrodynamic collision of two spheres. *J. Fluid Mech.* **163**, 479–497 (1986).
- Glasheen, J. W. & McMahon, T. A. Vertical water entry of disks at low Froude numbers. *Phys. Fluids* **8**, 2078–2083 (1996).
- Richardson, E. G. The impact of a solid on a liquid surface. *Proc. Phys. Soc.* **61**, 352–367 (1948).
- Brennen, C. E. *A Review of Added Mass and Fluid Inertial Forces* Report CR 82.010 (Naval Civil Engineering Laboratory, 1982).
- Liu, A. J. & Nagel, S. R. Jamming is not just cool any more. *Nature* **396**, 21–22 (1998).

**Supplementary Information** is linked to the online version of the paper at [www.nature.com/nature](http://www.nature.com/nature).

**Acknowledgements** We thank E. Brown, J. Burton, J. Ellowitz, Q. Guo, W. Irvine, M. Miskin, S. Nagel, C. Orellana, V. Vitelli, T. Witten and W. Zhang for discussions and J. Burton for his PIV code. This work was supported by NSF through its MRSEC programme (DMR-0820054) and by the US Army Research Office through grant number W911NF-12-1-0182. S.R.W. acknowledges support from a Millikan fellowship.

**Author Contributions** S.R.W. and H.M.J. conceived the study and wrote the paper. S.R.W. performed the experimental work, analysed results and created the model.

**Author Information** Reprints and permissions information is available at [www.nature.com/reprints](http://www.nature.com/reprints). The authors declare no competing financial interests. Readers are welcome to comment on the online version of this article at [www.nature.com/nature](http://www.nature.com/nature). Correspondence and requests for materials should be addressed to S.R.W. ([swaitukaitis@uchicago.edu](mailto:swaitukaitis@uchicago.edu)).